



HAL
open science

Microstructure and mechanical behavior of superelastic Ti-24Nb-0.5O and Ti-24Nb-0.5N biomedical alloys

A. Ramarolahy, Philippe Castany, F. Prima, P. Laheurte, Isabelle Péron,
Thierry Gloriant

► **To cite this version:**

A. Ramarolahy, Philippe Castany, F. Prima, P. Laheurte, Isabelle Péron, et al.. Microstructure and mechanical behavior of superelastic Ti-24Nb-0.5O and Ti-24Nb-0.5N biomedical alloys. *Journal of the mechanical behavior of biomedical materials*, 2012, 9, pp.83-90. 10.1016/j.jmbbm.2012.01.017 . hal-00926952

HAL Id: hal-00926952

<https://hal.science/hal-00926952>

Submitted on 10 Jan 2014

HAL is a multi-disciplinary open access archive for the deposit and dissemination of scientific research documents, whether they are published or not. The documents may come from teaching and research institutions in France or abroad, or from public or private research centers.

L'archive ouverte pluridisciplinaire **HAL**, est destinée au dépôt et à la diffusion de documents scientifiques de niveau recherche, publiés ou non, émanant des établissements d'enseignement et de recherche français ou étrangers, des laboratoires publics ou privés.

Microstructure and mechanical behavior of superelastic Ti–24Nb–0.5O and Ti–24Nb–0.5N biomedical alloys

A. Ramarolahy^a, P. Castany^a, F. Prima^b, P. Laheurte^c, I. Péron^a, T.
Gloriant^a,

^a INSA Rennes, UMR CNRS 6226 SCR / Chimie-Métallurgie, 20 avenue des Buttes
de Coësmes, 35708 Rennes cedex 7, France

^b ENSCP Paris, UMR CNRS 7045 Laboratoire de Physico-Chimie des Surface, 11 rue
Pierre et Marie Curie, 75231 Paris cedex 5, France

^c Université de Metz, UMR CNRS 7239 Laboratoire d'Etude des Microstructures et
Mécanique des Matériaux, Ile du Saulcy, 57045 Metz cedex, France

Abstract

In this study, the microstructure and the mechanical properties of two new biocompatible superelastic alloys, Ti–24Nb–0.5O and Ti–24Nb–0.5N (at.%), were investigated. Special attention was focused on the role of O and N addition on α'' formation, superelastic recovery and mechanical strength by comparison with the Ti–24Nb and Ti–26Nb (at.%) alloy compositions taken as references. Microstructures were characterized by optical microscopy, X-ray diffraction and transmission electron microscopy before and after deformation. The mechanical properties and the superelastic behavior were evaluated by conventional and cyclic tensile tests. High tensile strength, low Young's modulus, rather high superelastic recovery and excellent ductility were observed for both superelastic Ti–24Nb–0.5O and Ti–24Nb–0.5N alloys. Deformation twinning was shown to accommodate the plastic deformation in these alloys and only the $\{332\} \langle 113 \rangle$ twinning system was observed to be activated by electron backscattered diffraction analyses.

Keywords: Titanium alloys; Superelasticity; Stress induced martensite; Deformation twinning

1. Introduction

Titanium alloys are widely used as biomaterials due to their low density, good mechanical properties and biocompatibility (Geetha et al., 2009). A standard titanium biomaterial for orthopedic implants is the Ti-6Al-4V alloy, which was first developed for aeronautic applications. However, a perfectly biocompatible Ti-based alloy must be composed of non-cytotoxic elements. In Ti-6Al-4V, aluminium ions released from the implant are associated with long term health problems like neurological pathologies while vanadium oxide, V_2O_5 , is also known to be cytotoxic (Eisenbarth et al., 2004 and Williams, 2008). Moreover, the high Young's modulus of the Ti-6Al-4V alloy caused by the $\alpha+\beta$ microstructure affects long-term practical performance due to the stress shielding effect (Huiskes et al., 1992 and Niinomi et al., 2002). Since the β microstructure in titanium alloys exhibits a significantly lower modulus than the $\alpha+\beta$ microstructure, there is a tremendous scope for improvement in terms of alloy design for an ideal orthopedic implant. Consequently, a new generation of low modulus β -titanium alloys, which are free of vanadium and aluminium, have been made with β -stabilizing and biocompatible elements such as Nb, Ta and Zr (Laheurte et al., 2010 and Niinomi, 2008).

Among metastable β -titanium alloys, biocompatible Ti-Nb based alloys are very promising for biomedical applications. Indeed, these alloys possess a low elastic modulus closer to that of bone, which contributes to avoiding the harmful stress shielding phenomenon. On the other hand, promising shape memory effect and superelastic behavior can be achieved due to the α'' martensitic transformation (orthorhombic phase) occurring in these alloys. Consequently, Ni-free alloys can also be envisaged for biomedical smart devices such as coronary stents, orthopedic staples or orthodontic wires (Miyazaki et al., 2006 and Sun et al., 2010).

In the Ti-Nb binary system, it was reported that Ti-(22-25)Nb (at.%) alloys exhibit a shape memory effect while a superelastic behavior is observed in Ti-(25.5-27)Nb alloys (Kim et al., 2004 and Kim et al., 2006). For the specific Ti-24Nb composition, the α'' martensitic transformation start (M_s) was estimated to be at 338 K, which is consistent with the observation of a fully α'' microstructure at room temperature after water quenching from the β phase domain. It is well known that the superelastic behavior in β -titanium alloys results from the reversible stress-induced α'' martensitic transformation (SIM) from the parent β phase. Consequently, an initial fully β microstructure is needed to obtain a superelastic effect. This is typically the case for the Ti-26Nb alloy composition for which the critical stress inducing the

α'' martensitic transformation from β was observed at about 170 MPa by tensile testing (Kim et al., 2004).

In Ti–Nb alloys, formation of as-quenched α'' martensite can be inhibited by the addition of oxygen (Kim et al., 2005). For example, it was shown that addition of 1 at.% of O decreases M_s by about 160 K in the Ti–22Nb alloy composition. Furthermore, it was also recently shown that the formation of as-quenched α'' martensite is suppressed by adding oxygen in Ti–Nb–Ta–Zr (TNTZ) alloys (Besse et al., 2011). Similarly, formation of as-quenched α'' martensite was suppressed by addition of nitrogen in Ti–(18–24)Nb–4Zr–2Ta (at.%) (Tahara et al., 2010).

The objective of this work is to investigate the microstructure and the mechanical properties of two new biocompatible superelastic alloys containing oxygen and nitrogen: Ti–24Nb–0.5O and Ti–24Nb–0.5N (at.%). Special attention will be focused on the role of O and N addition on α'' formation, superelastic recovery and tensile strength by comparison with the Ti–24Nb and Ti–26Nb (at.%) alloy compositions taken as references.

In superelastic Ti–Nb based titanium alloys, large ductility is often observed due to various mechanisms of plastic deformation that can be activated depending on the composition and thus on the stability of the β phase. Indeed, in β -type alloys, plastic deformation can be accommodated by both dislocation slip and twinning (Hanada and Izumi, 1986, Furuhashi et al., 1992 and Bertrand et al., 2011). In this study, deformation twinning of the two superelastic Ti–24Nb–0.5X (X = O and N) alloys is more particularly investigated.

2. Experimental

Ti–24Nb, Ti–26Nb, Ti–24Nb–0.5O and Ti–24Nb–0.5N alloy compositions (at.%) were synthesized by the cold crucible levitation melting technique (CCLM) under high vacuum in this study. For the synthesis, ultra-pure raw metals, 99.999% pure titanium and 99.9% pure niobium were used, and oxygen and nitrogen were added by using 99.8% pure TiO₂ powder and 99.5% pure TiN powder, respectively. The CCLM process, which limits the contact between the melt and the cold copper crucible, was shown to be an efficient method to melt biocompatible Ti-based alloys possessing a high melting point and to obtain uniform chemical composition without contamination (Bertrand et al., 2010).

Ingots obtained from melting were next homogenized at 1223 K for 72 ks under high vacuum, followed by water quenching. The ingots were then cold rolled at room temperature until a 90% reduction in thickness was achieved. From this cold-rolled state, tensile specimens were

machined to obtain normalized shapes: 3 mm width, 0.5 mm in thickness and a gage length of 15 mm. The specimens were finally solution-treated in the β -phase domain at 1123 K for 1.8 ks under vacuum in order to restore a fully recrystallized microstructure from the cold-rolled state after water quenching.

The microstructures of the solution treated alloys were characterized by X-ray diffraction (XRD) with a Philips PW3710 diffractometer using Cu $K\alpha_1$ radiation ($\lambda=0.154060$ nm) and observed by optical microscopy (Leica, OM). Before observations, the samples were first mechanically polished on silicon carbide abrasive papers followed by a final polishing step with a colloidal silica suspension (particle size: 50 nm) and next chemically etched with a 5% HNO_3 , 5% HF and 90% H_2O solution (vol.%).

The mechanical properties were evaluated from conventional tensile tests until rupture carried out on an Instron 3369 machine with a strain rate of $10^{-4} s^{-1}$. An extensometer was used to precisely measure the deformation of the specimens. The superelastic behavior was characterized from cyclic tensile tests with strain increments of 0.5% followed by stress release up to an elongation of 5%. All tensile tests were performed with the tensile direction parallel to the rolling direction.

The microstructures after deformation of both Ti–24Nb–0.5O and Ti–24Nb–0.5N alloys were observed by electron backscattered diffraction (EBSD) in a scanning electron microscope (SEM) and by transmission electron microscopy (TEM). These observations were carried out on tensile specimens after being strained up to 6%. SEM–EBSD analyses were performed in a Jeol JSM 6400 microscope equipped with a TSL EBSD system. Surface samples were prepared by a similar route to the samples for optical microscopy. TEM observations were made using a JEOL 2000FX microscope operating at 200 kV. Specimens for TEM observations were prepared by a conventional twin-jet polishing technique.

3. Results and discussion

3.1. Microstructure

Fig. 1 shows typical optical micrographs displaying the microstructures of the four solution-treated alloys investigated in this study. The Ti–24Nb alloy (a) seems to present a dual phase microstructure, composed of equiaxed β grains with thin α'' martensite needles inside. On the contrary, the Ti–26Nb (b), Ti–24Nb–0.5O (c) and Ti–24Nb–0.5N (d) alloys seems to possess a fully β -grain microstructure with a grain dimension varying between a few tens and a few hundreds of micrometers. X-ray diffraction analyses carried out on each alloy are presented in

Fig. 2. The XRD pattern of the Ti–24Nb alloy confirms the presence of the self-accommodated α'' martensite (a), which composed the majority of the microstructure. However, a small amount of residual parent β phase was detected according to the relative intensities of the peaks of both phases. As only residual β phase is detected, the equiaxed microstructure observed by optical microscopy is thus the signature of the high temperature β phase microstructure due to the solution treatment, which was done in the β domain before quenching. From this XRD pattern, each α'' peak could be clearly identified and the cell parameters of this C-centered orthorhombic phase (space group: Cmcm) were determined and are reported in Table 1. The XRD patterns obtained from Ti–26Nb (b), Ti–24Nb–0.5O (c) and Ti–24Nb–0.5N (d) alloys show that these alloys present a β -phase microstructure with, however, a very small amount of residual α'' martensite phase in Ti–24Nb–0.5N. For the latter, a fully β microstructure can be considered but the martensite start is probably close to the room temperature. From the XRD patterns, the cell parameter for each body-centered cubic β -phase (space group: Im3m) was calculated and the values are presented in Table 1. This study clearly shows that the addition of O or N inhibits the formation of the self-accommodated α'' martensite during quenching. This effect was previously mentioned in binary Ti–Nb alloys when O is added (Kim et al., 2005) and this study shows a similar behavior with N addition. It is also worth noting that nitrogen is a weaker inhibitor of the α'' formation than oxygen. A small addition of O or N (0.5 at.%) is thus shown to be sufficient to modify the microstructure of the Ti–24Nb alloy from a near fully α'' microstructure into a fully β microstructure.

3.2. Tensile tests

Conventional and cyclic tensile tests were performed at room temperature to characterize the mechanical properties of the four alloys. The conventional tensile curves until rupture are presented in Fig. 3 and the cyclic tensile curves between 0% and 5% strain are presented in Fig. 4. All the mechanical characteristics determined in this study from tensile tests are reported in Table 2. In this table we also report the mechanical characteristics of the Ti–6Al–4V ELI alloy used in orthopedics (<http://www.aerospacemetals.com/titanium.html-10/2011>) and those reported from the literature concerning the solution-treated superelastic binary Ti–26Nb alloy (Kim et al., 2004).

The conventional tensile curves (Fig. 3) show an increase of both yield strength (black arrows) and ultimate tensile strength (white arrows) with the addition of O or N in

comparison with both binary Ti–24Nb and Ti–26Nb alloys. This strengthening is due to the fact that both O and N, as interstitial elements, are well known to involve a solid-solution hardening effect in alloys. As seen in Table 2, the yield and ultimate tensile strengths of both Ti–24Nb–0.5O and Ti–24Nb–0.5N alloys are considerably increased in comparison with the superelastic binary Ti–26Nb. The mechanical strength is almost two times higher in the case of the Ti–24Nb–0.5O alloy and reaches a similar order of magnitude in comparison with the orthopedic Ti–6Al–4V ELI alloy.

O and N are also usually known to decrease the ductility of alloys but in the present case the ductility seems not to be altered by the addition of interstitial elements by comparison with the binary Ti–26Nb alloy. In the case of the Ti–24Nb–0.5O alloy, the measured elongation at rupture (22%) exceeds even that of Ti–6Al–4V.

The Ti–24Nb, Ti–26Nb and Ti–24Nb–0.5N stress–strain curves show a double yielding behavior. As self-accommodated α'' martensite is present after quenching in Ti–24Nb, the plateau on the stress–strain curve of this alloy is mainly due to the reorientation of martensite variants. Concerning the Ti–26Nb and Ti–24Nb–0.5N alloys, as the microstructure is fully β , the plateau is due to the formation of α'' stress-induced martensite (SIM) during straining. A similar plateau induced by SIM transformation is also observed in the superelastic β Ti–26Nb alloy elaborated by Kim et al. (2004). On the contrary, the stress–strain curve of Ti–24Nb–0.5O does not possess such a plateau.

Oxygen is observed to possess a higher strengthening effect than nitrogen in this study. In fact, the strengthening is also dependent on the microstructure, as stress-induced martensitic transformation occurs in superelastic alloys. As previously mentioned, nitrogen was shown to be a weaker inhibitor of α'' formation than oxygen. Consequently, it can be supposed that the α'' formation intervening at lower stress in Ti–25Nb–0.5N limits the solid-solution hardening effect of N.

The Young's modulus values (incipient modulus defined by the slope of the tangent at zero stress) were found to be very low in this study: 50, 54 and 43 GPa for Ti–26Nb, Ti–24Nb–0.5O and Ti–24Nb–0.5N, respectively. Thus, these alloys possess elastic moduli approaching that of bone (~30 GPa) as is the case with many superelastic β -type Ti-based alloys. Consequently, addition of interstitial elements seems not to change the Young's modulus significantly. With this alloy family, the elastic modulus is often observed to be more than twice as low as that of Ti–6Al–4V alloy as is the case with the Ti–24Nb–0.5O and Ti–24Nb–0.5N alloys of the present study. It has to be mentioned that the excellent yield strength/elastic

modulus ratio (0.012) obtained for the Ti–24Nb–0.5O alloy is much higher than in the case of the Ti–6Al4V alloy (0.007). Consequently, this biocompatible Ti–24Nb–0.5O alloy, combining high strength, low modulus and good ductility, is very competitive with the Ti–6Al–4V alloy for use as bone substitute in orthopedics.

The superelastic behavior of the three Ti–26Nb, Ti–24Nb–0.5O and Ti–24Nb–0.5N alloys can be well characterized by cyclic tensile tests at room temperature. Superelastic recovery strains (ϵ_{se}) were measured at 3% strain (6th load–unload cycle) as shown in Fig. 4 and values are reported in Table 2. The measured ϵ_{se} values are found to be higher for both Ti–24Nb–0.5N (2%) and Ti–24Nb–0.5O (2.2%) alloys than for interstitial-free solution-treated β -type superelastic alloys. It is also confirmed by these cyclic tensile tests that Ti–26Nb and Ti–24Nb–0.5N possess a double yielding while Ti–24Nb–0.5O does not. The presence of a plateau for Ti–24Nb–0.5N is clearly due to the reversible SIM transformation as commonly observed in superelastic β -titanium alloys. In the present case, the critical stress inducing SIM transformation, σ_c , was evaluated to be at about 130 MPa (Fig. 4c), which is a rather low value, confirming that for this alloy the martensite start, M_s , is close to room temperature. For Ti–24Nb–0.5O, the absence of a plateau may suggest that no SIM transformation occurs in this alloy.

3.3. Microstructure after deformation

The two superelastic Ti–24Nb–0.5N and Ti–24Nb–0.5O alloys were observed by TEM on tensile specimens after being strained up to 6%. Fig. 5 shows a typical bright field TEM image (a) and the corresponding electron diffraction pattern (b) of the Ti–24Nb–0.5N microstructure after deformation. In the bright field image, the typical needle-like morphology of the α'' martensite phase is observed. The diffraction pattern exhibits typical diffraction spots related to the presence of both a body-centered cubic β matrix (higher intensity spot network) and C -centered orthorhombic α'' martensite needles (lower intensity spot network). This observation confirms that the plateau observed on the tensile curve for this alloy composition is definitely related to the stress-induced α'' martensitic transformation. Fig. 6 shows a typical bright field TEM image (a) and the corresponding electron diffraction pattern (b) representing the microstructure of the deformed Ti–24Nb–0.5O alloy. Once again, needle-like α'' martensitic precipitates are observed in β grains, which is confirmed in the related electron diffraction pattern. Consequently, although no plateau was observed on

tensile test, stress-induced martensite transformation is also a mechanism occurring in this Ti–24Nb–0.5O alloy composition as was the case with the Ti–24Nb–0.5N alloy.

A multifunctional β -type Ti–23Nb–0.7Ta–2Zr–1.2O alloy composition, called “gum metal”, showing a superelastic behavior without a plateau on tensile test, has been reported (Saito et al., 2003). It was claimed that this alloy deforms through unconventional dislocation-free mechanisms implying “giant faults” and stress-induced martensite was excluded from the deformation mechanisms. The fact that no SIM transformation occurs in “gum metal” was confirmed by our group in a recent study in which cyclic tensile tests and TEM observations were carried out (Besse et al., 2011).

In a recent work (Tahara et al., 2011), it was shown that the addition of 1 at.% O in a Ti–23Nb–1.0O (at.%) alloy composition produces nanosized modulated domains in the β matrix and it was suggested that these domains could suppress long-range martensitic transformation. In the Ti–24Nb–0.5O alloy composition, the oxygen content is half that of the “gum metal” composition. Consequently, the oxygen content in the present alloy is not high enough to suppress the martensitic transformation as this phase was clearly observed by TEM. In a recent work concerning Ti–24Nb–4Zr–8Sn–(0.08–0.40)O (wt%) alloys (Obbard et al., 2011), it was established that oxygen raises the critical stress required to induce martensitic transformation; in other word suppression of the martensitic transformation becomes stronger with increasing oxygen content. The absence of the plateau in Ti–24Nb–0.5O can thus be explained by the fact that the stress required to induce the martensite transformation is close to the yield strength situated at about 665 MPa. This hypothesis is confirmed by the existence of hysteresis between loading and unloading on the cyclic tensile curve (Fig. 4b). This behavior is typically characteristic of the reversible β/α'' transformation. In the “gum metal” alloy such hysteresis was not observed by cyclic tensile tests and perfect superimposition between loading and unloading was obtained (Besse et al., 2011). It has to be mentioned that hysteresis is still observed in the plastic domain in the present alloy, which constitutes an original behavior never reported in the literature.

In β -type Ti alloys, plastic deformation is known to be accommodated by dislocation glide and, in most cases, by twinning formation. Dislocation glide in a metastable β alloy has recently been studied by our group and dislocations were observed to glide in the $\{110\}, \{112\}$ or $\{123\}$ planes with $a/2 \langle 111 \rangle$ Burgers vectors by TEM (Castany et al., 2011).

Concerning the twinning formation, two twinning systems are commonly observed in metastable β titanium alloys: $\{112\} \langle 111 \rangle$ and $\{332\} \langle 113 \rangle$ (Hanada and Izumi, 1986 and Bertrand et al., 2011). In the present study, twinning formation in Ti–24Nb–0.5N and Ti–24Nb–0.5O alloys was more particularly investigated. For that, EBSD analyses were performed on the two alloys after tensile tests interrupted after 6% strain. The results are presented in Fig. 7.

In this figure, inverse pole figure maps ((a) and (c)) show that bands of a few micrometers in thickness inside the β grains were formed in both deformed Ti–24Nb–0.5N and Ti–24Nb–0.5O alloys. These bands correspond to mechanical twins intervening in both alloys. In some grains, two twin variants can be observed in the same grain. In Fig. 7, we also present examples of misorientation profiles (along the *AB* line) in each alloy ((b) and (d)). In all cases, the angle measurements between the parent grain and the twin were found to be about 50.5° . This misorientation corresponds to a $\Sigma 11$ CSL (coincidence site lattice) boundary characteristic of the $\{332\} \langle 113 \rangle$ twinning system. This twinning system was confirmed by analysis of common poles of the two crystals on 332 and 113 pole figures. Such analysis was carried out on several grains for the two investigated alloys and only $\{332\} \langle 113 \rangle$ twins were found.

Thus, the plastic deformation of the present superelastic alloys is accommodated by both dislocation glide and twinning. For the latter, only the $\{332\} \langle 113 \rangle$ twinning system was observed to be activated. Additionally, in the case of the Ti–24Nb–0.5O alloy, it seems that SIM also occurred in the plastic region. This point needs, however, to be elucidated and in-situ experiments are under development. All the deformation mechanisms occurring in superelastic Ti–24Nb–0.5N and Ti–24Nb–0.5O alloys contribute to the very good ductility observed.

4. Conclusion

In this study, the microstructure and the mechanical behavior of two new superelastic Ti–24Nb–0.5X (X = O, N) biomedical alloys were investigated.

By tensile tests, high mechanical strength, low Young's modulus and excellent ductility were observed for both β -type alloys. By cyclic tensile tests, superelastic behavior was evidenced and rather high superelastic recoveries were obtained. Tensile tests carried out on the Ti–24Nb–0.5N alloy clearly show a double yielding behavior due to the reversible stress-induced α'' martensitic transformation (SIM). In the Ti–24Nb–0.5O alloy, such a double yielding

behavior was not observed because the critical stress inducing the SIM transformation was shown to occur at a value close to the yield strength.

The plastic deformation of both alloys was shown to be accommodated by dislocation glide and twinning which contribute to the high ductility observed. For the latter, only the $\{332\} \langle 113 \rangle$ twinning system was observed to be activated.

All the properties obtained with these superelastic Ti–24Nb–0.5N and Ti–24Nb–0.5O alloys seem to be particularly useful for their use as implants or prostheses in medicine

Acknowledgment

This work was supported by the French National Research Agency (No. ANR 08MAPR 0017).

References

Bertrand, E., Gloriant, T., Gordin, D.M., Vasilescu, E., Drob, P., Vasilescu, C., Drob, S.I., 2010. Synthesis and characterisation of a new superelastic Ti–25Ta–25Nb biomedical alloy. *J. Mech. Behav. Biomed. Mater.* 3, 559-564.

Bertrand, E., Castany, P., Péron, I., Gloriant, T., 2011. Twinning system selection in a metastable beta-titanium alloy by Schmid factor analysis. *Scripta Mater.* 64, 1110-1113.

Besse, M., Castany, P., Gloriant, T., 2011. Mechanisms of deformation in Gum Metal TNTZ-O and TNTZ titanium alloys: a comparative study on the oxygen influence. *Acta Mater.* 59, 5982-5988.

Castany, P., Besse, M., Gloriant, T., 2011. Dislocation mobility in gum metal beta-titanium alloy studied via in situ transmission electron microscopy. *Phys. Rev. B.* 84, 020201.

Eisenbarth, E., Velten, D., Müller, M., Thull, R., Breme, J., 2004. Biocompatibility of β -stabilizing elements of titanium alloys. *Biomater.* 25, 5705-5713.

Furuhara, T., Nakamori, H., Maki, T., 1992. Crystallography of alpha precipitated on dislocations and deformation twin boundaries in a beta titanium alloy. *Mater. Trans. JIM*. 33, 585-595.

Geetha, M., Singh, A.K., Asokamani, R., Gogia, A.K., 2009. Ti based biomaterials, the ultimate choice for orthopaedic implants - A review. *Prog. Mater. Sci.* 54; 397-425.

Hanada, S., Izumi, O., 1986. Transmission electron-microscopic observations of mechanical twinning in metastable beta titanium alloys. *Metall. Trans. A*. 17, 1409-1420.

Huiskes, R., Weinans, H., Vanrietbergen, B., 1992. The relationship between stress shielding and bone-resorption around total hip stems and the effects of flexible materials. *Clin. Orthop. Relat. Res.* 274, 124-134.

Kim, H.Y., Satoru, H., Kim, J.I., Hosoda, H., Miyazaki, S., 2004. Mechanical properties and shape memory behavior of Ti-Nb alloys. *Mater. Trans.* 45, 2443-2448.

Kim, J.I., Kim, H.Y., Hosoda, H., Miyazaki, S., 2005. Shape memory behavior of Ti-22Nb-(0.5-2.0)O (at%) biomedical alloys. *Mater. Trans.* 46, 852-857.

Kim, H.Y., Ikehara, Y., Kim, J.I., Hosoda, H., Miyazaki, S., 2006. Martensitic transformation, shape memory effect and superelasticity of Ti-Nb binary alloys. *Acta Mater.* 54, 2419-2429.

Laheurte, P., Prima, F., Eberhardt, A., Gloriant, T., Wary, M., Patoor, E., 2010. Mechanical properties of low modulus beta titanium alloys designed from the electronic approach. *J. Mech. Behav. Biomed. Mater.* 3, 565-573.

Miyazaki, S., Kim, H.Y., Hosoda, H., 2006. Development and characterization of Ni-free Ti-base shape memory and superelastic alloys. *Mater. Sci. Eng.* A438-440, 18-24.

Niinomi, M., Hattori, T., Morikawa, K., Kasuga, T., Suzuki, A., Fukui, H., Niwa, S., 2002. Development of low rigidity β -type titanium alloy for biomedical applications. *Mater. Trans.* 43, 2970-2977.

Niinomi, M., 2008. Mechanical biocompatibilities of titanium alloys for biomedical applications. *J. Mech. Behav. Biomed. Mater.* 1, 30-42.

Obbard, E.G, Hao, Y.L., Talling, R.J., Li, S.J., Zhang, Y.W., Dye, D., Yang, R., 2011. The effect of oxygen on alpha" martensite and superelasticity in Ti-24Nb-4Zr-8Sn. *Acta Mater.* 59, 112-125.

Saito, T., Furuta, T., Hwang, J.H., Kuramoto, S., Nishino, K., Suzuki, N., Chen, R., Yamada, A., Ito, K., Seno, Y., Nonaka, T., Ikehata, H., Nagasako, N., Iwamoto, C., Ikuhara, Y., Sakuma, T., 2003. Multifunctional alloys obtained via a dislocation-free plastic deformation mechanism. *Science* 300, 464-467.

Sun, F., Nowak, S., Gloriant, T., Laheurte, P., Eberhardt, A., Prima, F., 2010. Influence of a short thermal treatment on the superelastic properties of a titanium-based alloy. *Scripta Mater.* 63, 1053-1056.

Tahara, M., Kim, H.Y., Hosoda, H., Nam, T.H., Miyazaki, S., 2010. Effect of nitrogen addition and annealing temperature on superelastic properties of Ti-Nb-Zr-Ta alloys. *Mater. Sci. Eng. A527*, 6844-6852.

Tahara, M., Kim, H.Y., Inamura, T., Hosoda, H., Miyazaki, S., 2011. Lattice modulation and superelasticity in oxygen-added β -Ti alloys. *Acta Mater.* 59, 6208-6218.

Williams, D., 2008. On the mechanisms of biocompatibility. *Biomater.* 29, 2941-2953.

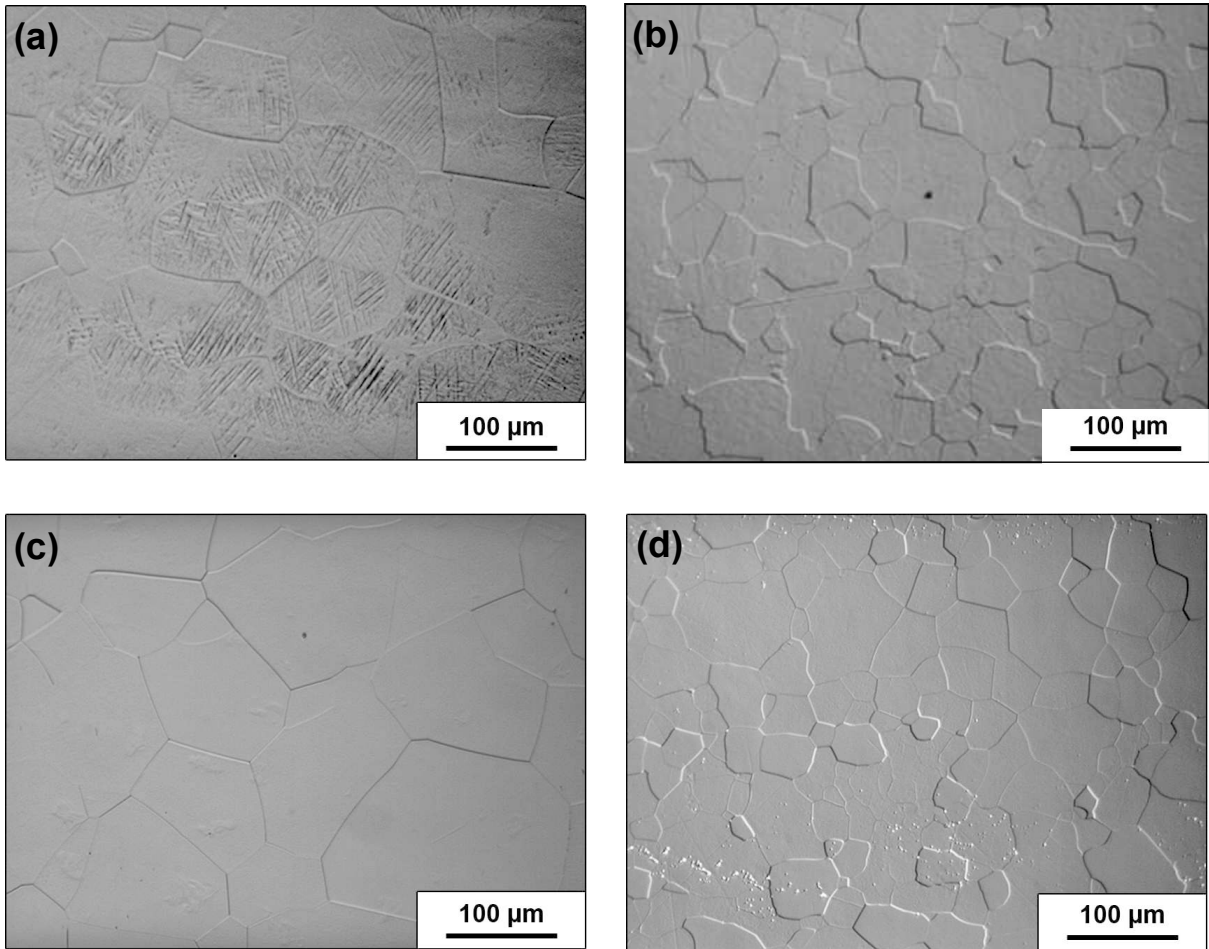


Fig. 1. Optical micrographs of the solution-treated Ti-24Nb (a), Ti-26Nb (b), Ti-24Nb-0.5O (c), and Ti-24Nb-0.5N (d) alloys, respectively.

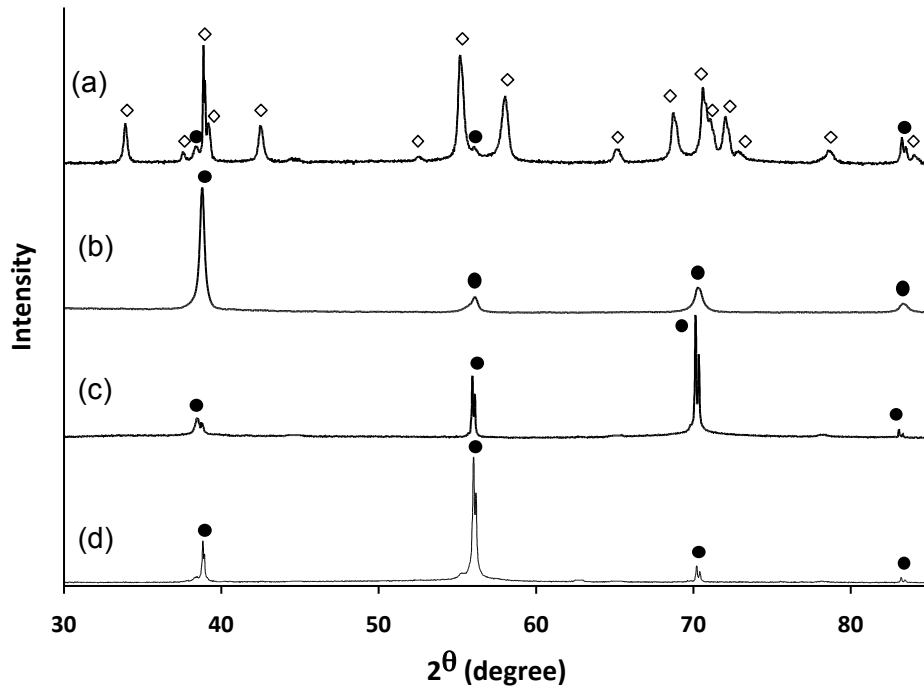


Fig. 2. X-ray diffraction profiles of the solution-treated Ti-24Nb (a), Ti-26Nb (b), Ti-24Nb-0.5O (c), and Ti-24Nb-0.5N (d) alloys, respectively. The closed symbol (\bullet) corresponds to the parent β (cubic) phase and open symbol (\diamond) corresponds to the martensite α'' (orthorhombic) phase.

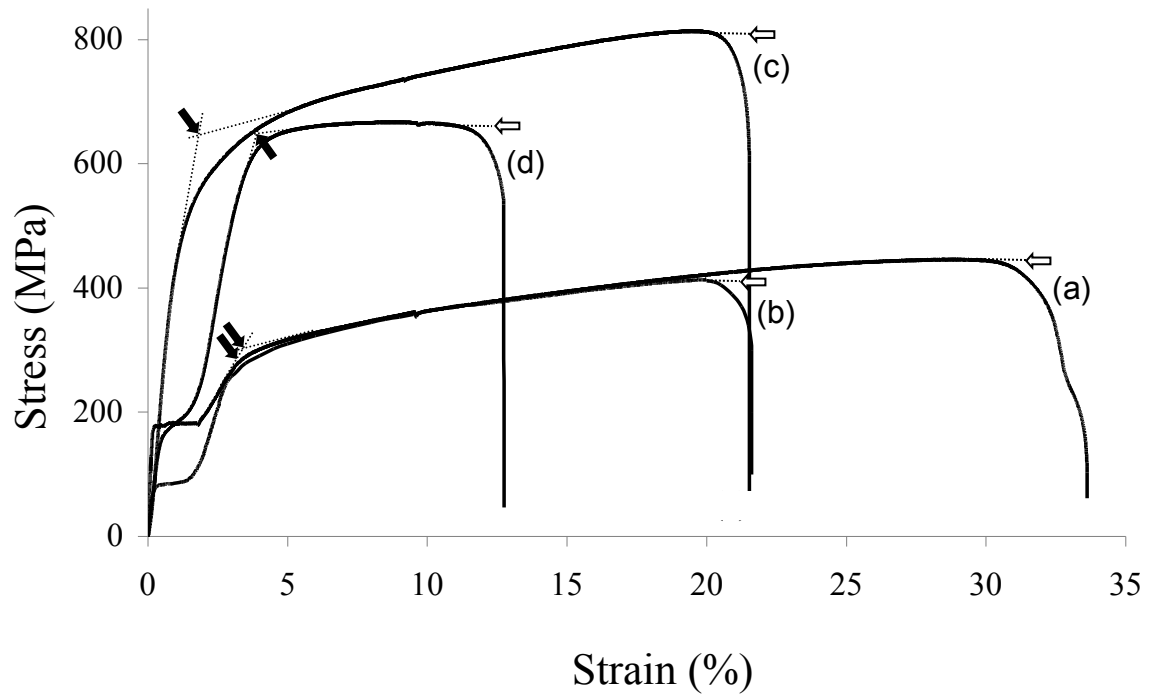


Fig. 3. Conventional stress–strain curves of Ti–24Nb (a), Ti–26Nb (b), Ti–24Nb–0.5O (c), and Ti–24Nb–0.5N (d) alloys at room temperature.

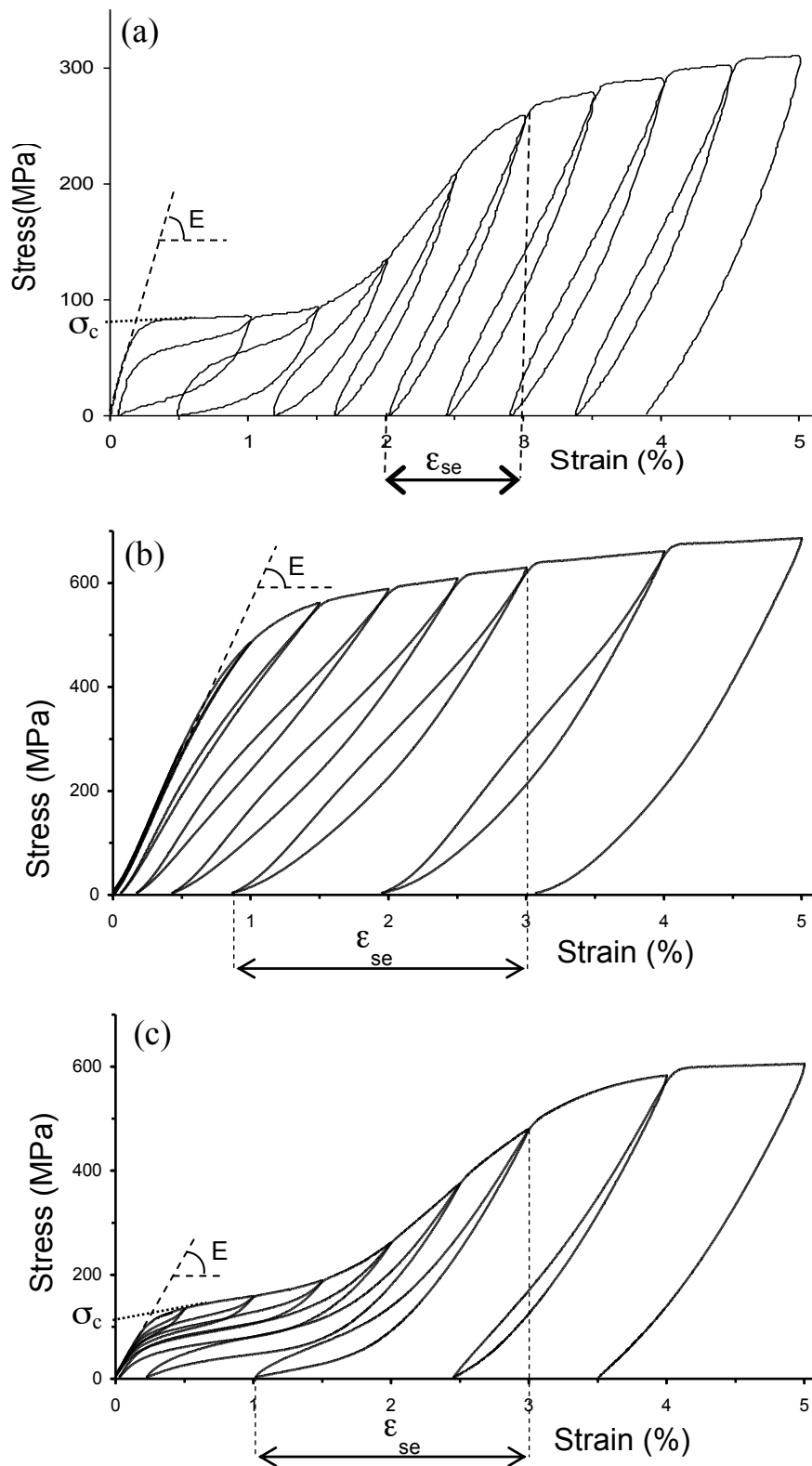


Fig. 4. Cyclic stress–strain curves of superelastic Ti–26Nb (a), Ti–24Nb–0.5O (b) and Ti–24Nb–0.5N (c) alloys at room temperature.

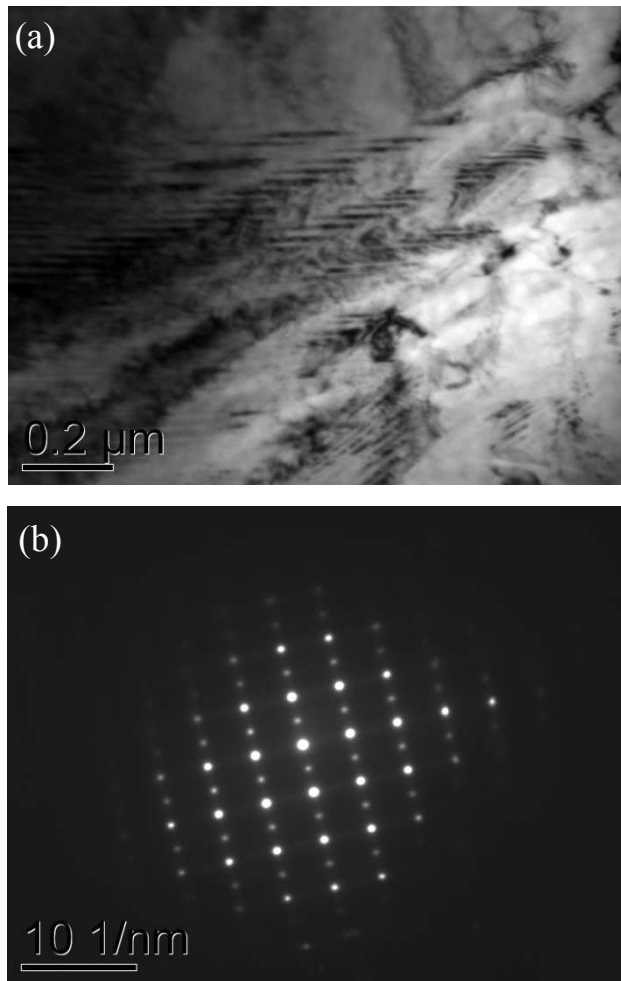


Fig. 5. Typical bright-field TEM image (a) and the corresponding electron diffraction pattern ($[100]_{\beta}$ zone axis) (b) from the deformed Ti-24Nb-0.5N alloy.

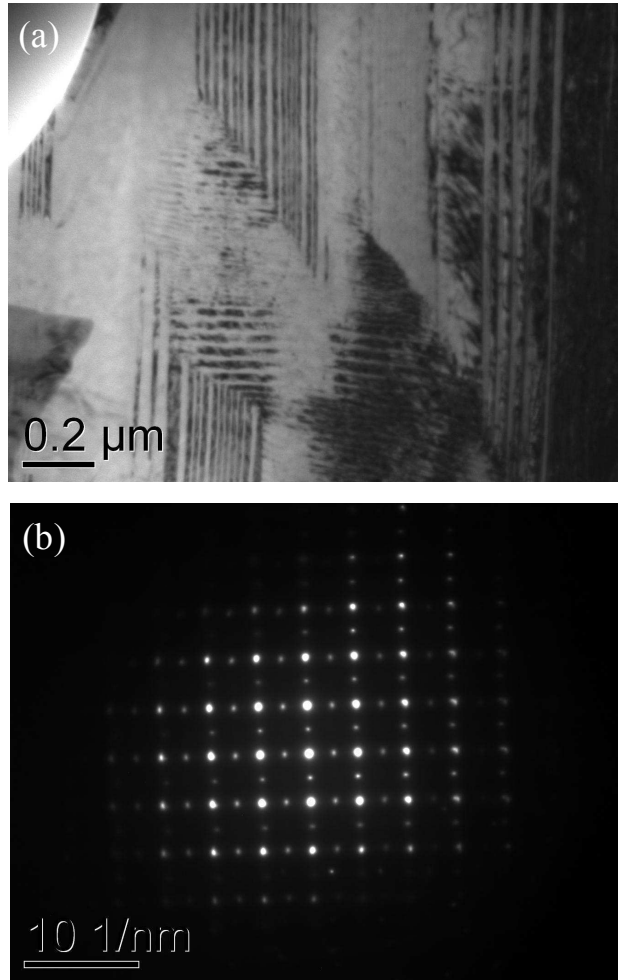


Fig. 6. Typical bright-field TEM image (a) and the corresponding electron diffraction pattern ($[100]_{\beta}$ zone axis) (b) from the deformed Ti-24Nb-0.5O alloy.

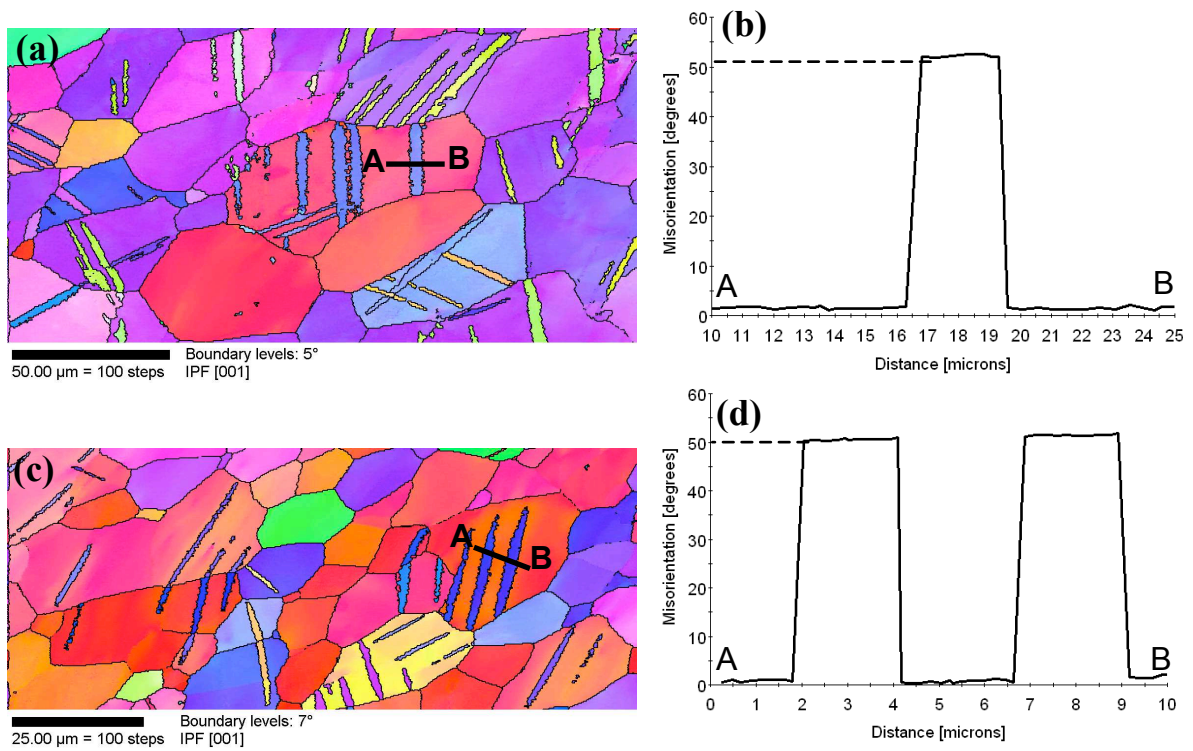


Fig. 7. EBSD analyses after 6% of deformation. Typical inverse pole figure maps from Ti-24Nb-0.5O (a) and Ti-24Nb-0.5N (c) alloys. Parts (b) and (d) show the profiles of misorientation (along the *AB* line) in each alloy, respectively.

Table 1. Microstructure and lattice parameters of the β (cubic) and α'' (orthorhombic) phases in Ti-24Nb, Ti-26Nb, Ti-24Nb-0.5O and Ti-24Nb-0.5N alloys.

Alloys (at %)	Phases	Lattice parameters (nm)			
		Parent (β)	Martensite (α'')		
		a_{β}	$a_{\alpha''}$	$b_{\alpha''}$	$c_{\alpha''}$
Ti-24Nb	near fully α''	-	0.31752	0.47879	0.46339
Ti-26Nb	β	0.32786	-	-	-
Ti-24Nb-0.5O	β	0.32882	-	-	-
Ti-24Nb-0.5N	β	0.32837	-	-	-

Table 2. Mechanical properties of the studied Ti–24Nb, Ti–26Nb, Ti–24Nb–0.5O and Ti–24Nb–0.5N alloys. Mechanical characteristics (from the literature) of the Ti–6Al–4V ELI alloy and the solution-treated superelastic Ti–26Nb alloy are also indicated.

Alloys	YS [MPa]	UTS [MPa]	ER [%]	E [GPa]	ϵ_e (or ϵ_{se}) [%]	σ_c [MPa]
Ti-24Nb (α'')	300	445	33	60	0.5	no SIM
Ti-26Nb (β) <i>this work</i>	290	420	22	50	1 (ϵ_{se})	80
Ti-24Nb-0.5O (β)	665	810	22	54	2.2 (ϵ_{se})	?
Ti-24Nb-0.5N (β)	665	665	13	43	2 (ϵ_{se})	130
Ti-6Al-4V ELI ($\alpha+\beta$)	790	860	15	114	0.7	no SIM
Ti-26Nb (β) <i>from Kim et al., 2004</i>	350	420	17	50	1.5 (ϵ_{se})	170

YS : yield strength *UTS* : ultimate tensile strength *ER* : elongation at rupture

E : Young's modulus ϵ_e (or ϵ_{se}) : elastic (or superelastic) recovery σ_c : critical SIM stress